Journal of Modern Physics, 2024, 15, 1485-1501
https://www.scirp.org/journal/jmp
ISSN Online: 2153-120X
ISSN Print: 2153-1196

DFT Studies of Electronic Properties and Effect of He and Xe Incorporation in Selected Ceramics

Barbara Szpunar[1]*, Jayangani I. Ranasinghe[1], Jerzy A. Szpunar[2]

[1]Department of Physics and Engineering Physics, University of Saskatchewan, Saskatoon, Canada
[2]Department of Mechanical Engineering, University of Saskatchewan, Saskatoon, Canada
Email: *B.Szpunar@usask.ca

How to cite this paper: Szpunar, B., Ranasinghe, J. I., & Szpunar, J. A. (2024) DFT Studies of Electronic Properties and Effect of He and Xe Incorporation in Selected Ceramics. *Journal of Modern Physics*, **15**, 1485-1501.
https://doi.org/10.4236/jmp.2024.1510061

Received: July 16, 2024
Accepted: September 11, 2024
Published: September 14, 2024

Abstract

The electronic properties of several prospective nuclear fuels are not yet well known. We used Quantum Espresso and EPW codes to evaluate the electron density of states, the electronic heat capacity coefficient, the electron-phonon coupling strength, the number of mobility electrons, and the electronic heat conductivity. The electronic properties for ThN, ThC and UN using a slightly different approach that were previously evaluated are discussed and the results are compared. We confirmed that while the electronic heat capacity coefficient is linearly dependent on the electron density of states at Fermi energy, such a simple relation could not be used to determine the difference in the electronic heat conductivity of investigated materials. The highest heat conductivity was registered in ThN. These metallic fuels also have high U/Th density, therefore are more economical since enrichment is expensive. Furthermore, it is important to examine swelling in these high-density fuels. We evaluated that UN had 42% more U atoms per unit volume than UO_2 and a 55% higher volume increase when accommodating one Xe atom in one interstitial of a $(2 \times 2 \times 2)$ supercell. However, for He, the volume increase was 27% lower in UN. Interestingly, even though the Th atom's density in ThN and ThC was lower than that of U atoms in the UN compound, a similar trend of volume changes was found. We concluded, therefore, that when we consider swelling, the local structural symmetry (tetrahedral versus octahedral sites) is more important than the density of atoms. The 37 % greater of absolute value of the total energy increase due to incorporation of Xe in ThC versus ThN cannot be explained by the crystal structure since a ThC-Xe supercell has a higher lattice constant than a ThN-Xe corresponding supercell. Such results can only be explained by investigating electronic structure.

Keywords

UN, ThN, ThC, Thermal Conductivity, Defects

1. Introduction

Metallic ceramic fuels are very interesting materials as their thermal conductivity remains high even at very high temperatures due to significant electronic heat transport. They are important because urania fuel, which is used in conventional nuclear reactors, is not the optimum option for some designs of new generation reactors due to its low thermal conductivity [1]. High-density metallic compounds uranium silicide (U_3Si_2), and uranium and thorium nitrides (UN, ThN) [2], have been proposed [3] for implementation in future reactors. In previous papers [4]-[6], we focused on UN, which has the same cubic structure ($Fm\bar{3}m$ symmetry) as ThN and ThC. Furthermore, we compared ThN, ThC, and UN in recent papers [7]-[9].

Measurements of porosity-free ThN [10] showed a large total thermal conductivity at room temperature of 55.4 $Wm^{-1}K^{-1}$, but no analysis of electronic contribution was made. Moreover, as discussed in reference [7], the previously used argument that since ThN has about an 8 times lower density of states than UN at Fermi energy therefore it should have poorer electrical and thermal conductivities [11] is incorrect. That statement also contradicts recent experimental results [10]. To clarify the differences in the reported values of thermal conductivity, first-principles calculations of the electronic transport were made, and a detailed theoretical analysis was used to identify the origin of such differences and was reported [7]-[9]. In this work we intend to compare and analyze the results obtained previously in [6] [8] [9] with a different method of evaluation for electronic carriers.

The discussed metallic fuels also have high U and Th density, therefore are more economical since enrichment is expensive. We evaluated that UN had 42% more U atoms per unit volume than UO_2. Furthermore, it is important to examine swelling in these high-density fuels. In particular, a comparison between volume expansion and energetics when these fuels are accommodating two fission gases of different atomic sizes, such as He and Xe, is useful. The needed and important evaluation of differences between swelling in these metallic ceramic fuels versus traditionally used urania are presented here.

2. Methodology

First-principles, predictive calculations based on density functional theory (DFT) as implemented in Quantum ESPRESSO (QE) code were used with the plane-wave-method [12].

We evaluated structural properties and energetics of selected metallic fuels and Urania. The norm-conserved pseudopotentials with the functional for solids developed for generalized gradient approximation (GGA) of the Perdew, Burke, and Ernzerhof (PBEsol) [13] were used here in studying energetics and volume expansion when He and Xe are incorporated in tetrahedral interstitials of ThN, ThC and UN, and octahedral interstitials in Urania. The local density approximation (LDA) [14] was used to calculate the energy of isolated single atoms of He and Xe, in a box with 1nm length to prevent interaction. The formation energy of these fission products gases (atom X) in interstitial ($\Delta E_{\text{int}}^{F}$) was calculated as a difference of the total energy of the compound with one atom X placed in the interstitial minus sum of energy of the pure compound (E) and the energy of isolated atom E^{X}:

$$\Delta E_{\text{int}}^{F} = E_{\text{int}}^{X} - \left(E + E^{X}\right) \tag{1}$$

Furthermore the respective % of volume increase (%ΔV_{int}) and % of the total absolute value of energy increase (%ΔE_{int}) during this incorporation was calculated.

Additionally, we compared the previously evaluated [6] [8] [9] electronic properties for ThN, ThC and UN using a slightly different approach in obtaining the number of electronic carriers. In the previous QE calculations, for ThN and ThC the GGA of the Perdew, Burke, and Ernzerhof functional (PBE) [15] was used as implemented in QE code [12], while the functional for solids developed for GGA of the Perdew, Burke, and Ernzerhof (PBEsol) [13] was used in studying UN. We are limited here to non-spinpolarised calculation because of restrictions within EPW code [16]. Additionally, the solver for Boltzmann transport equations (BTE) is incorporated only in the most recent version (v. 5.4) of EPW code. This code was used to calculate resistivity and number of electronic carriers [9] in contrast to early calculations where experimental resistivity was used [6] [8]. Furthermore, a simplified solution of BTE is also provided in EPW code [16] to compute the electrical resistivity ($\rho_{calc}(T)$) up to 1000 K. It uses the well-known Ziman's formula [17] for metals (Eq. 54 in Ref. [16]) with the Eliashberg transport coupling function: $\alpha_{tr}^{2}F(\omega)$ (Eq. 55 in Ref. [16]):

$$\rho_{calc}(T) = \frac{4\pi m_e}{ne^2 k_B T} \times \int_0^\infty \mathrm{d}\omega\hbar\omega\alpha_{tr}^{2}F(\omega)n(\omega,T)\left[1+n(\omega,T)\right] \tag{2}$$

where k_B is the Boltzmann constant, m_e and e are the mass and charge of an electron, T is the temperature in K, $n = nc/\Omega$ with nc being the number of mobility electrons per unit cell (Ω), and $n(\omega, T)$ is the Bose-Einstein distribution with the integral carried over the energy.

The electronic number of carriers (n) in Eq. 2 is a parameter that can be calculated either by using experimental resistivity or derived from a solution of BTE in EPW code. This parameter has been evaluated previously [5] [6] [8] using experimental data and since it is slightly temperature dependent, an average of its value between 300 K and 1000 K has been chosen as a characteristic parameter for ThN, ThC, and UN. Similarly, an average value of the number of electronic carriers has been evaluated from theoretical values of resistivity calculated using BTE in EPW code as shown in [9].

The other important property is the electronic contribution to the thermal conductivity (κ_e) and it can be calculated via the Wiedemann-Franz law [18] from the electrical conductivity (σ) or from resistivity ($\rho(T) = \sigma(T)^{-1}$):

$$\kappa_e = \frac{\pi}{3}\left(\frac{k_B}{e}\right)^2 \sigma T \tag{3}$$

The integrated electron-phonon (e-ph) coupling strength (λ) as a function of frequency (ω) has been calculated previously [8] for ThN, UN, and ThC using QE v6.7 from:

$$\lambda = \int_0^{\omega} \frac{\alpha^2 F(\omega)}{\omega} \mathrm{d}\omega \tag{4}$$

It is used here together with the other parameters such as the electron density of states at Fermi energy $n(\varepsilon_F)$ and the electronic specific heat coefficient (γ) to analyze differences in the electronic transport of heat in ThN, UN, and ThC. The formula for the electronic heat capacity coefficient is given below:

$$\gamma = \pi/3 \times 6.242 \times 10^{18} n(\varepsilon_F) N_A k_B^2 \tag{5}$$

3. Results and Discussion

3.1. Crystal Structure

The ground state equilibrium structure was evaluated using QE code. We assumed electronic configurations of $5f^3$, $6d^1$, $7s^2$ for U, $5f^0$, $6d^2$, $7s^2$ for Th, $2s^2$, $2p^4$ for O, $2s^2$, $2p^3$ for N and $2s^2$, $2p^2$ for C atoms. The conjugate gradient diagonalization was used, and the following parameters were applied: Methfessel-Paxton (MP) smearing; a mixing beta parameter of 0.15 in Broyden charge density mixing; a convergence threshold of 10 - 12 Ry. We adopted the kinetic cutoff energies determined previously for the norm-conserved pseudopotentials of 250 Ry (3401 eV) for thorium compounds [8] [9] [19] and 150 Ry (2041 eV) for U compounds [5] [9]. ThN, ThC, UN and UO_2 have cubic structures ($Fm\bar{3}m$) with cations (U, Th) forming stable fcc type frames. U atoms in UO_2 are surrounded by eight O atoms in tetrahedral positions while octahedral interstitials are not occupied. In contrast, in the metallic fuels discussed here, U and Th have four nearest neighbours (O or N) in octahedral positions while tetrahedral interstitials are not occupied.

In **Table 1**, for each compound listed in column one, the U/Th atomic density is shown in column two as evaluated using equilibrium lattice constants calculated with implementation in the QE GGA-PBEsol functional and listed in column three. The previously calculated lattice constants [8] [9] using GGA-PBE are shown in column four while experimental results are listed in the last column. We find a very good agreement between the calculated and measured values.

The results in **Table 1**, column two, confirm that UN has 42% more U atoms per unit volume than UO_2. Therefore, UN is more economical since it will require lower enrichment, which is expensive. ThN and ThC also show a higher density of Th atoms than the calculated U atom density in UO_2.

3.2. He and Xe Incorporation

We demonstrated in Section 3.1 that the metallic ceramic fuels investigated here have higher U/Th atom density than traditionally used Urania. Therefore, it is important to evaluate if this leads to enhanced fuel swelling.

Table 1. The calculations for compounds listed in column one are shown as indicated in the first row: U/Th atomic density in column two as evaluated using equilibrium lattice constants calculated using the QE GGA-PBEsol functional and listed in column three. The previously calculated lattice constants [8] [9] using GGA-PBE are shown in column four, while experimental results are listed in the last column together with reference numbers.

Compound	Density	a (GGA-PBEsol)	a (GGA-PBE)	a (experimental)
	U/Th atoms/vol (nm^3)	nm	nm	nm
UN	34.1415	0.4893		0.489 [20]
ThN	28.6931	0.5185	0.5161 [8] [9]	0.5167 [21] 0.5160 [10]
ThC	26.1766	0.5346	0.5336 [8] [9]	0.5342 [22]
UO_2	24.1035	0.5495		0.547127 [23]

We investigated here the effect of incorporating He and Xe in one interstitial in (2 × 2 × 2) supercells as illustrated in Figures 1 and Figures 2 respectively for UO_2 and UN. Both He and Xe atoms were incorporated in each compound separately. All supercells have the same number (32) of U/Th atoms. The supercell for UO_2-He is shown in Figure 1: It contains 32 U atoms and 64 O atoms and one He placed in an octahedral interstitial site.

We present in Figure 2 an exemplary picture of the supercells used for all metallic ceramic compounds with 64 atoms total and one Xe atom incorporated in a tetrahedral site (0.25, 0.25, 0.25).

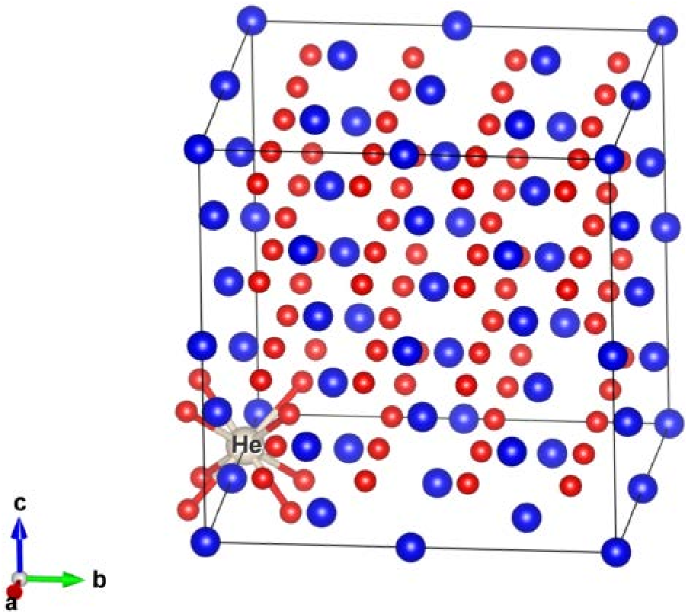

Figure 1. Exemplary supercell of UO_2 with a total of 96 atoms plus one He atom in the octahedral interstitial site (0.5, 0.0, 0.0). 64 O and 32 U atoms are shown as red and blue balls, respectively.

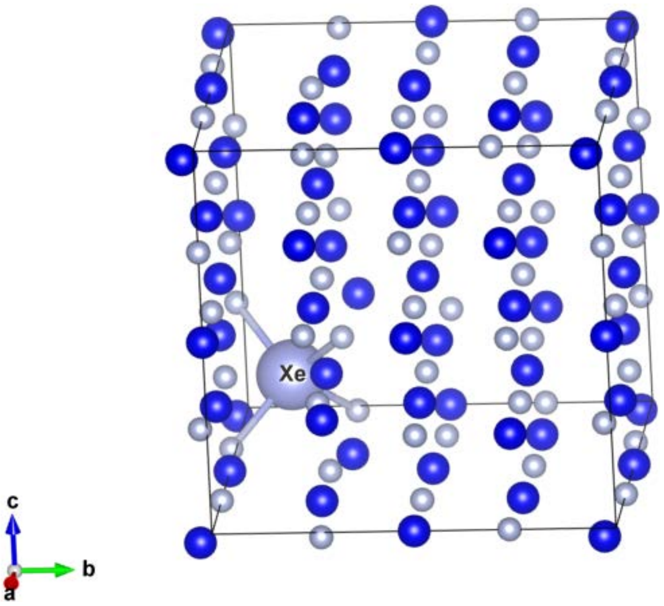

Figure 2. Exemplary supercell of metallic ceramic compound: UN with 32 U and 32 N atoms indicated by blue and grey balls respectively. The one Xe atom in a tetrahedral interstitial (0.25, 0.25, 0.25).is also shown.

In Table 2, column two, the calculated lattice constants of the respective supercells listed in column one are shown. The respective formation energies ($\Delta E_{\text{int}}^{F}$) as evaluated from Eq. 1 for incorporated He and Xe atoms in interstitials are shown in the last column. The formation energy decreases linearly ($R^2 = 0.999$ for Xe and 0.954 for He) with increasing lattice constants and it is up to three times

Table 2. The calculated lattice constants (a) for the supercells listed in column one are shown in column two and the respective formation energies ($\Delta E_{\text{int}}^{F}$) are shown in the last column The evaluated distances between incorporated He/Xe atoms in the interstitial sites to their nearest neighbour (O/N) and the nearest U/Th atoms are shown in columns three and four, respectively.

Compound	a (calculated)	Distance [nm]	Distance [nm]	$\Delta E_{\text{int}}^{F}$ in interst.
	[nm]	O/N-interst. (He/Xe)	Interst. (He/Xe) to U/Th	eV
UN-He	0.4898	0.2160	0.2203	8.2441
UN-Xe	0.4946	0.2456	0.2700	18.8777
ThN-He	0.5191	0.2269	0.2337	4.0495
ThN-Xe	0.5245	0.2593	0.2755	13.0997
ThC-He	0.5352	0.2372	0.2377	3.6239
ThC-Xe	0.5403	0.2606	0.2788	10.4799
UO_2-He	0.5503	0.2378	0.2771	0.3882
UO_2-Xe	0.5534	0.2562	0.2908	7.6515

larger for incorporation of Xe than for He atoms. Additionally, the evaluated distances between incorporated He/Xe atoms in interstitial sites (0.25, 0.25, 0.25). to their nearest neighbour (O/N) and the nearest U/Th atoms are shown in columns three and four, respectively.

In **Figure 3(a)**, the percentage volume increases due to incorporation of He (grey circles) or Xe (dark blue squares) are shown as a function of the lattice constants of the respective supercells (2a) with the indicated name of the pure compound. Incorporation of FP in UO_2 has been extensively studied in magnetic and nongnetic states using various functionals as reviewed in [24]. Hybrid functionals were used for comparison to study incorporation of FP in interstitial [24]. However due to usage of small conventional unit cells for these computationally demanding functional the respective percentage volume increases were three times larger than evaluated here for (2 × 2 × 2) supercells when incorporating He (0.43% versus 1.2%.) and Xe (2.12% versus 6.90%). GGA+U was used to evaluate FP incorporation in antiferromagnetic (AFM) UN in ref. [25] therefore unphysical tetragonal distortion was observed. The studied here non magnetic (NM) cases and previous research on UO_2 with noncolinear magnetism [26] have found stable cubic structures in agreement with experiment. Alternatively UN with ferromagnetic (FM) ordering is also cubic and since it is a weak magnetism the evaluated formation energies for Xe in interstitials in UN AFM and FM only differed by 0.3% [27]. The volume expansion was not presented for UN in ref. [25] but elastic correction for (2 × 2 × 2) supercells for He and Xe incorporation in interstitials was found to be small (1% for He and 5.5% for Xe). The difference between energy incorporation for He and Xe in UN was close to the found here difference between the formation energies (11.66 eV [25] versus 12.27 eV). We confirm here that UN had 42% more U atoms per unit volume than UO_2 and a 55% higher volume increase when accommodating one Xe atom in one interstitial site of a (2 × 2 × 2) supercell. However, for He, the volume increase was 27% lower in UN, which can be explained by having lower number of nearest neighbor (NN) atoms (four N versus eight O). The previous evaluation [28] confirmed that going beyond GGA/LDA approximation or using spin polarized calculations was not necessary to evaluate structural properties of UC with defects and the found lattice constant change using GGA (PBE) of UC with incorporation of FP are very close to evaluated here for He (small −0.1% versus 0.1 %) and Xe (1.2% versus 1.1%) in ThC. The differences between formation energies of Xe and He calculated previously [28] and evaluated here differences for the respective formation energies are comparable (9.09 eV versus 6.86 eV). Interestingly, even though the Th atoms' density in ThN and ThC was lower than that of U atoms in the UN compound, a similar trend was found in volume increase when incorporating Xe atoms (**Figure 3(a)**). In contrast, a lower percentage volume increase was observed in UO_2 (12%). We conclude, therefore, that for swelling, the local structural symmetry (tetrahedral versus octahedral sites) is more important than the density of atoms.

The percentage of energy increase (E pure compound) when incorporating He or Xe atoms in interstitials is presented in Figure 3(b). The energy change for small He atoms is very small, and it is almost the same for tetrahedral interstitials of the considered metallic ceramic fuels. It is only slightly lower for incorporation into octahedral interstitial in UO_2. In contrast, the % the total absolute value of energy change of a larger gaseous atom, such as Xe, varies a lot and it is also much higher. ThC has the lowest binding energy and the percentage energy increases to a very high value (Figure 3(b)) where it is about four times higher than the percentage energy increase for positioning Xe in an octahedral site of UO_2. The 37 % higher total absolute value of energy increase for ThC versus ThN cannot be explained by crystal geometry since the ThC-Xe supercell has a higher lattice constant (Table 2, second column) than the ThN-Xe supercell. This can only be explained by investigating electronic structure, as discussed in Section 3.3.

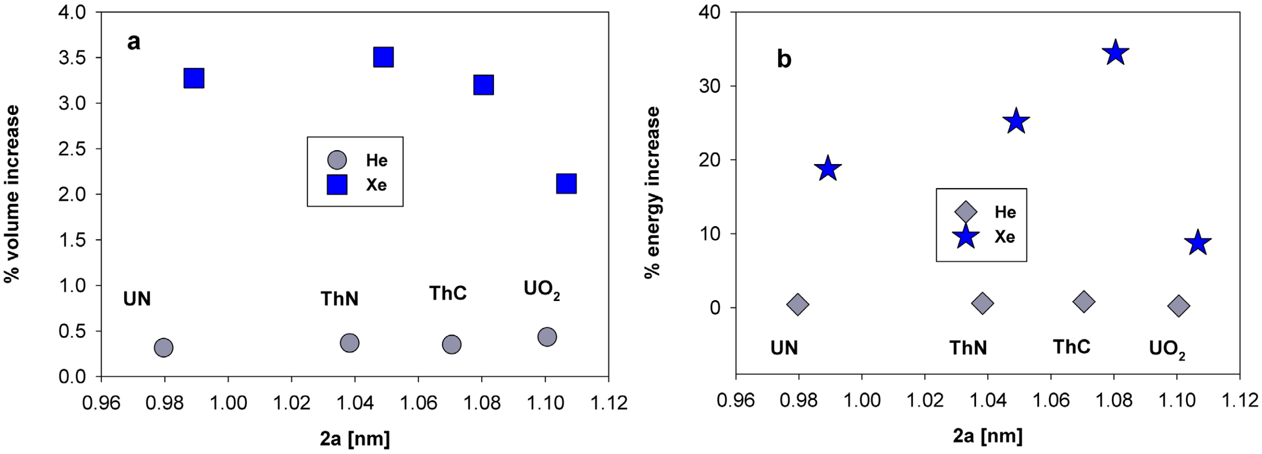

Figure 3. The calculated a: % volume increase for the respective incorporation of He (grey spheres) and Xe (dark blue squares) as a function of superlattice lattice constants with indicated corresponding compounds, and b: % of absolute value of the total energy increase (Eq. 1) for the respective incorporation of He (grey diamonds) and Xe (dark blue stars) as a function of superlattice lattice constants with indicated corresponding compounds.

3.3. The Effect of He and Xe on Electronic Structure

In previous work, we studied the electronic structure of UN in detail [5] and we also compared the electronic structure of ThN with ThC [8]. In this work, we compare the effect on electronic structure of neighbouring atoms: small He atoms compared with much larger Xe atoms whose ground state gaseous neutral electronic configuration is: [Kr] $4d^{10}$, $5s^2$, $5p^6$. In current calculations we use $1s^2$ electrons for He and $4d^{10}$, $5s^2$, $5p^6$ electrons for Xe. They are incorporated in one interstitial site in supercells as shown in Figures 1 and Figures 2. In an octahedral interstitial of UO_2 they are surrounded by eight nearest neighbours (NN) of O atoms (Figure 1) while in tetrahedral position they have four nearest neighbours: N atoms in UN (Figure 2) and ThN, and C atoms in ThC. The electrons included in the calculations from NN atoms are $2s^2$ and 2p with occupations varying from 4 to 2 for O, N and C, respectively.

In Figure 4 we show the respective electron densities of states of He and Xe together with their nearest neighbours' (NN) electron densities of states of 2s and 2p electrons. To analyse the effect of interaction, we also plot electron densities of

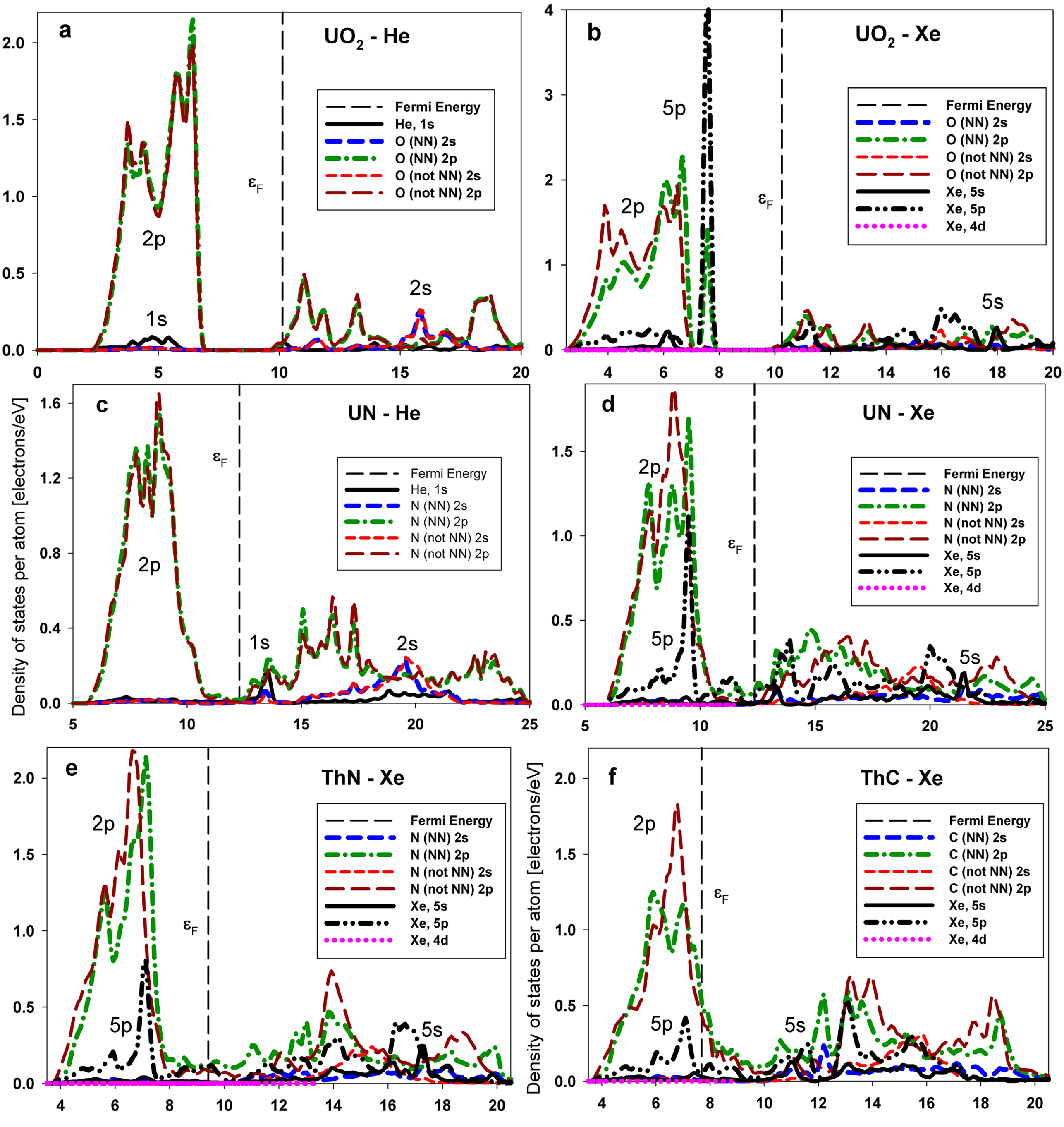

Figure 4. The electron densities of states of incorporated He and Xe atoms in a, b: UO$_2$, c, d: UN, e: ThN, f: ThC and its influence on the next nearest neighbour (NN) atom (O, N, C) is shown as indicated. The respective electron density (2s and 2p) of O, N and C atoms, which are not nearest neighbours (not NN) to either He or Xe, are shown for comparison.

states of O, N and C atoms, which are positioned away from He and Xe atoms (not NN) in the supercells. Figures 4(a) and Figures 4(c) illustrate that there is no visible interaction between 1s electrons of He (solid black line) with 2p electrons (dashed dot green line) of either O atoms in UO$_2$ or N atoms in UN. Only 2s electrons are slightly affected. This explains why incorporation of He into interstitials requires low energy as shown (grey diamonds) in Figure 3(b).

In contrast, incorporation of Xe atoms demonstrates (Figures 4(b), Figures 4(d), Figures 4(e), Figures 4(f)) strong interaction between 5p electrons (dashed dot dot dark blue line) of Xe and 2p electrons (dashed dot green line) of O, N and C.

Figures 4(b) illustrates that 5p electrons with a sharp single peak are almost unperturbed by the Xe atom positioned in an octahedral interstitial of UO_2. However, the lower energy peak of the 2p electron density of states of a NN O atom is depressed and higher energy peaks are enhanced, which leads to the net energy increase. Furthermore, the interaction between 2p electrons of NN atoms and 5p electrons of Xe incorporated in a tetrahedral interstitial in UN (Figures 4(d)) becomes more significant with the broadening of the 5p electron density of states. The density of states of 2p electrons of NN O (dashed dot green line) shows a three peaks structure with the largest value at higher energies than the single peak shape of 2p electron density of states of not NN O (dashed brown line) electrons. N and C have fewer 2p electrons (three and two versus four); therefore 5p electrons shown in Figures 4(e) and Figures 4(f) occupy a wide range of energies and 2p electrons are modified having an additional peak at energies where the peak of the 5p electron density of states is. These states are at higher energies, and it explains why % increase of absolute value of the total energy due to incorporation of Xe atom increases in ThN and especially in ThC versus UO_2.

The presented results demonstrate of importance of DFT studies in evaluating the effect of FP on swelling and energy increase. The comparison of behaviour of various ceramics using the same methodology (DFT Quantum Espresso Code) is particularly useful. Our work complements existing research which usually focus on one compound as discussed above.

Our analysis demonstrate that behaviour of FP is complex and DFT calculations are needed. Furthermore we need to note that swelling in nuclear fuel is a complex phenomena and requires inclusion of interaction of various defects and diffusion. Molecular dynamics studies with a large number of atoms and a very accurate potentials based on DFT are very promising as presented in recent work [26] [29].

3.4. Electronic Transport

ThN and ThC have similar crystal structures, as discussed above, but similarly to the energetics evaluated above, the electronic transport is significantly affected by the lower number (2 versus 3) of 2p electrons in C than in N atoms. The electronic properties for ThN, ThC and UN, using a slightly different approach, were previously evaluated [6] [8] [9] as discussed in Section 2, and we compare the results here. We used QE [12] and EPW [16] codes and found significant differences in electronic transport due to differences in the electronic structure of these compounds.

We compare the total electron density of states at Fermi energy ($n(\varepsilon_F)$), the electronic heat capacity coefficient (γ), and the electron-phonon coupling strength (λ) in Table 3. The shown averages were calculated over the temperature range 300 - 1000 K for the number of mobility electrons ($N_e\ (av)$), and the evaluated electronic heat conductivity (κ_e) for UN, ThN and ThC at a typical fuel surface temperature of 700

K. $N_e(av)$ values were obtained from experimental resistivity (exp) and from the solution of BTE using EPW code, as indicated, respectively. We summarized in Section 2 the methods used and the details of the calculations in our recent works [8] [9].

Table 3. The comparison of the electron density of states at Fermi energy ($n(\varepsilon_F)$), the electronic heat capacity coefficient (γ), the electron-phonon coupling strength (λ,) the average (over the temperature range 300 - 1000 K) the number of mobility electrons ($N_e(av)$ derived from experimental resistivity (exp. ρ) and EPW (BTE) code), and the electronic heat conductivity (κ_e(700 K)) of UN, ThN and ThC.

Calc. QE	UN	ThN	ThC
$n(\varepsilon_F)$ [electr./eV]	7.472	1.225	1.020
γ [J mol^{-1} K^{-2}]	0.0176 (0.006 (scaled))	0.00289	0.00240
λ	0.25	0.43	0.89
N_e (av), exp. ρ	0.34	2.76	1.20
N_e (av), EPW (BTE)	0.79	3.04	1.42
κ_e(700 K) [Wm^{-1}K^{-1}], exp. ρ	9.8	40.3	7.6
κ_e(700 K) [Wm^{-1}K^{-1}], EPW (BTE)	28.0 (10.5 (scaled))	38.2	14.7

We found that most of the calculated parameters are similar for both ThN and ThC except for the number of mobility electrons, which we found to be much higher in ThN (2.76 versus 1.20 as calculated from experimental resistivity or 3.04 versus 1.42 obtained using a solution from BTE). We also determined that electron-phonon coupling is about twice as high (0.89 versus 0.43) for ThC as for ThN. This results in ThN's high electronic thermal conductivity of 40.3 Wm^{-1}K^{-1} as evaluated using Eq. 2 or 38.2 Wm^{-1}K^{-1} as calculated from BTE and Eq. 3, respectively. Therefore, ThN is currently considered for application in nuclear reactors as its high thermal conductivity allows for fast heat dissipation and that makes reactors safer and more economical in operation.

We need to point out that the previously calculated values [8] for both the electron density of states $n(\varepsilon_F)$ and the electronic heat capacity coefficient (γ), as shown in **Table 3**, are very similar and rather smaller: $n(\varepsilon_F)$ in ThN is 1.225 versus 1.020 in ThC and (γ) in ThN is 0.00289 versus 0.00240 for ThC. However, it is incorrect to conclude that therefore electronic heat conductivity is low in both compounds as stated previously [11]. ThN has about four times higher electronic thermal conductivity than ThC, as shown in **Table 3**. Electronic heat conductivity is a transport phenomenon that is dependent on the number of mobile electronic carriers (N_e (av)) and e-ph scattering rate (λ) as discussed previously [6]-[9].

The calculations for non-magnetic UN predict a much higher electron density of states at Fermi Energy and heat capacity coefficient than for thorium compounds, as shown in **Table 3** and noted previously [6] [9]. There is also a lower number of electronic carriers in UN (0.34) as evaluated from experimental resistivity measurements, but lower electron-phonon coupling (0.25) still leads to a higher calculated electronic thermal conductivity for UN than for ThC as shown in **Table 3**. It is again important to note (**Table 3**) that while the electronic heat capacity coefficient is linearly dependent on the electron density of states at Fermi energy, this simple relation cannot be used to determine the electronic heat conductivity. However since UN is not NM but paramagnetic with non zero local moment we calculated the scaling factor equal to the ratio of the electron density of states at Fermi energy for NM and FM state ($s = DOS_{NM}(E_F)/DOS_{FM}(E_F)/ = 2.67$). We included in the bracket in **Table 3** a scaled conductivity by this factor at 700 K (10.5 $Wm^{-1}K^{-1}$).

In the current version 5.4 of EPW code, only electrons within 3/2 k_BT region around Fermi energy are assumed to be involved in electronic transport. Therefore, as evaluated from BTE, non-magnetic UN has high electronic thermal conductivity [9] as indicated by the red dashed-dot-dot line (28.0 $Wm^{-1}K^{-1}$ at 700 K), as shown in **Figure 5**. This does not agree with the experiment (red dashed-dot line [30]). The generalization of EPW calculations for UN with any magnetic ordering (ferromagnetic or antiferromagnetic) and a paramagnetic state, in contrast to a non-magnetic state, would lead to a much lower electron density of states of U atoms around Fermi Energy as shown previously [4], which would rectify these results. Note that in this work, for evaluation of the effect of incorporated FP atoms we analysed DOS close to non-U atoms, so therefore our evaluation is not affected by this discrepancy.

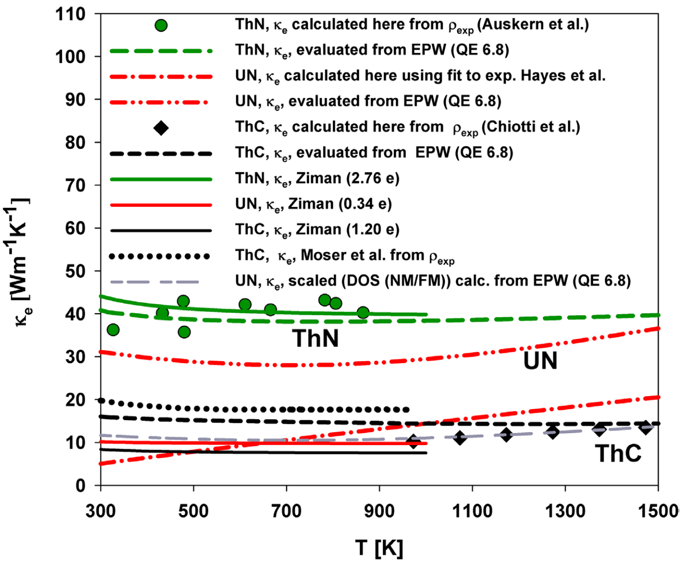

Figure 5. The electronic thermal conductivity (κ_e) of ThN, UN, and ThC, as calculated here from the experimental values for electrical resistivity via Wiedemann-Franz law (Eq. 3), are shown as green circles [31], dashed-dot red line [30], black diamonds [32], and doted black line [33], respectively. The calculated electronic thermal conductivities of ThN, UN, and ThC using Eq. 3 and the evaluated by EPW (BTE) electrical conductivity [9] are indicated by a medium-dashed green line, red dashed-dot-dot line, and black short-dashed line, respectively. κ_e calculated using Eqs. 2 and 3 are shown for the temperature range from 300 - 1000 K by solid lines: ThN, thin green, UN, medium red, ThC, thick black, respectively, as calculated previously [8]. The scaled by factor s ($s = 2.67$) the evaluated by EPW (BTE) thermal electrical conductivity of UN is indicated by grey short-long dashed line.

The electronic thermal conductivity (κ_e) of ThN and ThC as calculated from the experimental values for electrical resistivity via Wiedemann-Franz law [18] (Eq. 3) are shown in **Figure 5** as green circles [31], and black diamonds [32], dotted black line [33], respectively. They are in good agreement with the electronic thermal conductivities, calculated using Eq. 3, of non-magnetic ThN and ThC and evaluated by EPW (BTE) electrical conductivity [9] as indicated by a medium-dashed green line, and short-dashed black line, respectively. The agreement is particularly good for ThN. According to this prediction, UN should have lower electronic thermal conductivity than ThN, and the values obtained (red dashed-dot-dot line) are closer to the experimental data for ThN than for UN (red dashed dot line). ThN is non-magnetic and the assumption regarding electrons in UN that was incorrect as described above, was used in the calculations for UN. Therefore we also show in **Figure 5** as grey short-long dashed line the scaled by the factor s = 2.67 the evaluated by EPW (BTE) thermal electrical conductivity of UN.

Additionally, the values of κ_e calculated using Eqs. 2 and 3 with the averaged over temperature the number of electronic carriers evaluated from the experimental resistivity as calculated previously [8] are shown in **Figure 5** for the temperature range from 300 K - 1000 K (note not varying much with temperature) by solid lines, respectively for ThN, thin green, UN, medium red, ThC, thick black. They are in qualitative agreement with the experiment. Furthermore, the results from BTE calculations used together with Eq. 3 correctly predict that the κ_e of ThN is higher than for ThC as calculated from the first principles. It is important to note that the difference originates from the electronic shell structures of ThN and ThC. This results in a different affinity of 2p electrons in the half-filled shell of N ($2p^3$) versus the less than half-filled respective shell of C ($2p^2$) as discussed before [7] [8] and which leads to the different number of mobility electrons, as shown in **Table 3**. Furthermore, more experimental attempts should be made to separate the electronic and thermal conductivities in these metallic ceramic fuels. The preliminary evaluation of the electronic thermal conductivity of ThN using “alloy separation” and “curve fitting” techniques gives κ_e~40 $Wm^{-1}K^{-1}$ at 300 K (Fig. 41 of [34]) and this result supports our predictions of high electronic thermal conductivity in ThN, which remains almost insensitive to the temperature above 300 K (**Figure 5**). It has also been confirmed previously [19] that thermal conductivity remains relatively flat at the temperature interval 130 - 300 K.

It is now well established that although magnetic ordering in uranium compounds disappears at low temperature the local moment does not. The accurate calculations for uranium compound must include the effect of local magnetic moments on DOS and noncolinear magnetism like for example in ref. [26] for UO_2 to prevent artificial distortion like observed in [25].

4. Summary and Conclusions

The metallic fuels investigated here have high U/Th density and therefore are more economical since enrichment is expensive. We performed non-spin polarized calculations using QE consistent with EPW code capabilities.

It is important to examine effect of FP incorporation in these high-density fuels and especially compare ThN and ThC versus UN and UO_2, which have been much more extensively studied using various methods (e.g., [26] [27] [29] [35]). Similarly to this study, it has been confirmed [29] that the behaviour of fission gases is complex and require development of accurate potentials based on DFT calculations.

We showed that the calculated formation energies ($\Delta E_{\text{int}}^{F}$) for incorporated He and Xe atoms in interstitials decrease linearly with increasing lattice constants and it is up to three times larger for incorporation of Xe than for He atoms. However % of absolute value of the total energy increase due to incorporation of Xe and He is more complex.

The 37 % of absolute value of the total energy increase due to incorporation of Xe for ThC versus ThN cannot be explained by geometry since the ThC-Xe supercell has a higher lattice constant than the ThN-Xe supercell. Such differences were explained by investigating electronic structure.

We evaluated that UN has 42% more U atoms per unit volume than UO_2 and also has a 55% higher volume increase when accommodating one Xe atom in one interstitial of a (2 × 2 × 2) supercell. However, for He, the volume increase was 27% lower in UN. Interestingly, even though the Th atom's density in ThN and ThC was lower than that of U atoms in the UN compound, a similar trend was found. We concluded, therefore, that for swelling, the local structural symmetry (tetrahedral versus octahedral sites) was more important than the density of atoms.

We have demonstrated that electronic thermal conductivity can be evaluated in a very good agreement with experimental values using the first-principles calculation for ThN and in qualitative agreement for ThC. However, non-magnetic calculations predict that the electronic thermal conductivity of UN is too high, and resembles more the experimental data obtained for ThN than that of UN.

Our analysis shows that a high thermal conductivity of ThN is related to a high number of mobility electrons and low electron-phonon coupling strength. More experimental data for both ThN and ThC would be helpful for further analysis of the observed drastic differences in the electronic transport in these compounds with the same crystalline structure.

Acknowledgements

The authors acknowledge access to high-performance supercomputers at the Digital Research Alliance of Canada (CalculQuebec, WestGrid, and SHARCNET). Free access to Quantum Espresso and EPW codes with technical support (especially prompt installation of QE 6.8 by Ali Kerrache) is acknowledged. The first author acknowledges a constructive discussion with Dr. S. Poncé and a very helpful 2021 EPW workshop. This work was supported by a Discovery Grant from the National Sciences and Engineering Research Council of Canada.

Credit Author Statement

Barbara Szpunar: Investigation, Software, Calculations, Writing; Jayangani I. Ranasinghe: Conceptualization, Software; Jerzy A. Szpunar: Reviewing and Editing.

Conflicts of Interest

The authors declare that they have no known competing financial interests or personal relationships that could have appeared to influence the work reported in this paper.

References

[1] Pioro, I.L., Khan, M., Hopps, V., Jacobs, C., Patkunam, R., Gopaul, S., *et al.* (2008) SCW Pressure-Channel Nuclear Reactor Some Design Features. *Journal of Power and Energy Systems*, **2**, 874-888. https://doi.org/10.1299/jpes.2.874

[2] Gorton, J.P., Collins, B.S., Nelson, A.T. and Brown, N.R. (2019) Reactor Performance and Safety Characteristics of ThN-UN Fuel Concepts in a PWR. *Nuclear Engineering and Design*, **355**, 110317. https://doi.org/10.1016/j.nucengdes.2019.110317

[3] NEA (2018) State-of-the-Art Report on Light Water Reactor Accident-Tolerant Fuels. Nuclear Science, OECD Publishing.

[4] Szpunar, B. and Szpunar, J.A. (2014) Thermal Conductivity of Uranium Nitride and Carbide. *International Journal of Nuclear Energy*, **2014**, Article 178360. https://doi.org/10.1155/2014/178360

[5] Szpunar, B., Ranasinghe, J.I., Malakkal, L. and Szpunar, J.A. (2020) First Principles Investigation of Thermal Transport of Uranium Mononitride. *Journal of Physics and Chemistry of Solids*, **146**, Article 109636. https://doi.org/10.1016/j.jpcs.2020.109636

[6] Szpunar, B., Ranasinghe, J.I. and Szpunar, J.A. (2021) Electronic Transport of Uranium Mononitride. *Journal of Modern Physics*, **12**, 1349-1357. https://doi.org/10.4236/jmp.2021.1210084

[7] Szpunar, B., Ranasinghe, J.I., Malakkal, L. and Szpunar, J.A. (2021) First Principles Investigation of Thermal Properties of Thorium Mononitride. *Journal of Alloys and Compounds*, **879**, Article 160467. https://doi.org/10.1016/j.jallcom.2021.160467

[8] Szpunar, B., Ranasinghe, J.I., Szpunar, J.A. and Malakkal, L. (2022) Comparison of the Electronic Transport of ThN against ThC. *Journal of Physics and Chemistry of Solids*, **165**, Article 110647. https://doi.org/10.1016/j.jpcs.2022.110647

[9] Szpunar, B. (2022) First Principles Investigation of the Electronic-Thermal Transport of ThN, UN, and ThC. *Nuclear Materials and Energy*, **32**, Article 101212. https://doi.org/10.1016/j.nme.2022.101212

[10] Parker, S.S., White, J.T., Hosemann, P. and Nelson, A.T. (2019) Thermophysical Properties of Thorium Mononitride from 298 to 1700 K. *Journal of Nuclear Materials*, **526**, Article 151760. https://doi.org/10.1016/j.jnucmat.2019.151760

[11] Modak, P. and Verma, A.K. (2011) First-Principles Investigation of Electronic, Vibrational, Elastic, and Structural Properties of ThN and UN up to 100 GPa. *Physical Review B*, **84**, Article 024108. https://doi.org/10.1103/physrevb.84.024108

[12] Giannozzi, P., Baroni, S., Bonini, N., Calandra, M., Car, R., Cavazzoni, C., *et al.* (2009) QUANTUM ESPRESSO: A Modular and Open-Source Software Project for Quantum Simulations of Materials. *Journal of Physics: Condensed Matter*, **21**, Article 395502. https://doi.org/10.1088/0953-8984/21/39/395502

[13] Perdew, J.P., Ruzsinszky, A., Csonka, G.I., Vydrov, O.A., Scuseria, G.E., Constantin, L.A., *et al.* (2009) Erratum: Restoring the Density-Gradient Expansion for Exchange in Solids and Surfaces [phys. Rev. Lett.**100**, 136406 (2008)]. *Physical Review Letters*, **102**, Article 039902. https://doi.org/10.1103/physrevlett.102.039902

[14] Ceperley, D.M. and Alder, B.J. (1980) Ground State of the Electron Gas by a Stochastic Method. *Physical Review Letters*, **45**, 566-569. https://doi.org/10.1103/physrevlett.45.566

[15] Perdew, J.P., Burke, K. and Ernzerhof, M. (1996) Generalized Gradient Approximation Made Simple. *Physical Review Letters*, **77**, 3865-3868. https://doi.org/10.1103/physrevlett.77.3865

[16] Poncé, S., Margine, E.R., Verdi, C. and Giustino, F. (2016) EPW: Electron-Phonon Coupling, Transport and Superconducting Properties Using Maximally Localized Wannier Functions. *Computer Physics Communications*, **209**, 116-133. https://doi.org/10.1016/j.cpc.2016.07.028

[17] Ziman, J. (1960) Electrons and Phonons. Oxford University Press.

[18] Franz, R. and Wiedemann, G. (1853) Ueber die Wärme-Leitungsfähigkeit der Metalle. *Annalen der Physik*, **165**, 497-531. https://doi.org/10.1002/andp.18531650802

[19] Pérez Daroca, D., Llois, A.M. and Mosca, H.O. (2016) Point Defects in Thorium Nitride: A First-Principles Study. *Journal of Nuclear Materials*, **480**, 1-6. https://doi.org/10.1016/j.jnucmat.2016.07.057

[20] Knott, H.W., Lander, G.H., Mueller, M.H. and Vogt, O. (1980) Search for Lattice Distortions in UN, UAs, and USb at Low Temperatures. *Physical Review B*, **21**, 4159-4165. https://doi.org/10.1103/physrevb.21.4159

[21] Gerward, L., Olsen, J.S., Benedict, U., *et al.* (1988) Bulk Moduli and High-Pressure Phases of ThX Compounds. I. The Thorium Monopnictides. *High Temperatures-High Pressures*, **20**, 545-552.

[22] Street, R.S. and Waters, T.N. (1962) The Thermal Expansion of ThC and ThN. Energy Research Establishment, Harwell.

[23] Leinders, G., Cardinaels, T., Binnemans, K. and Verwerft, M. (2015) Accurate Lattice Parameter Measurements of Stoichiometric Uranium Dioxide. *Journal of Nuclear Materials*, **459**, 135-142. https://doi.org/10.1016/j.jnucmat.2015.01.029

[24] Ma, L. and Ray, A.K. (2012) Formation Energies and Swelling of Uranium Dioxide by Point Defects. *Physics Letters A*, **376**, 1499-1505. https://doi.org/10.1016/j.physleta.2012.03.017

[25] Claisse, A., Klipfel, M., Lindbom, N., Freyss, M. and Olsson, P. (2016) GGA+U Study of Uranium Mononitride: A Comparison of the U-Ramping and Occupation Matrix Schemes and Incorporation Energies of Fission Products. *Journal of Nuclear Materials*, **478**, 119-124. https://doi.org/10.1016/j.jnucmat.2016.06.007

[26] Dubois, E.T., Tranchida, J., Bouchet, J. and Maillet, J. (2024) Atomistic Simulations of Nuclear Fuel UO_2 with Machine Learning Interatomic Potentials. *Physical Review Materials*, **8**, Article 025402. https://doi.org/10.1103/physrevmaterials.8.025402

[27] Yang, L. and Kaltsoyannis, N. (2021) Incorporation of Kr and Xe in Uranium Mononitride: A Density Functional Theory Study. *The Journal of Physical Chemistry C*, **125**, 26999-27008. https://doi.org/10.1021/acs.jpcc.1c08523

[28] Freyss, M. (2010) First-Principles Study of Uranium Carbide: Accommodation of Point Defects and of Helium, Xenon, and Oxygen Impurities. *Physical Review B*, **81**, Article 014101. https://doi.org/10.1103/physrevb.81.014101

[29] Kocevski, V., Cooper, M.W.D., Claisse, A.J. and Andersson, D.A. (2022) Development and Application of a Uranium Mononitride (UN) Potential: Thermomechanical Properties and Xe Diffusion. *Journal of Nuclear Materials*, **562**, Article 153553. https://doi.org/10.1016/j.jnucmat.2022.153553

[30] Hayes, S.L., Thomas, J.K. and Peddicord, K.L. (1990) Material Property Correlations for Uranium Mononitride. *Journal of Nuclear Materials*, **171**, 289-299. https://doi.org/10.1016/0022-3115(90)90376-x

[31] Auskern, A.B. and Aronson, S. (1967) Electrical Properties of Thorium Nitrides. *Journal of Physics and Chemistry of Solids*, **28**, 1069-1071. https://doi.org/10.1016/0022-3697(67)90224-7

[32] Chiotti, P., Korbitz, F.W. and Dooley, G.J. (1967) Electrical Resistivity and Phase Relations for the Thorium-Carbon System. *Journal of Nuclear Materials*, **23**, 55-67. https://doi.org/10.1016/0022-3115(67)90131-6

[33] Moser, J.B. and Kruger, O.L. (1967) Thermal Conductivity and Heat Capacity of the Monocarbide, Monophosphide, and Monosulfide of Uranium. *Journal of Applied Physics*, **38**, 3215-3222. https://doi.org/10.1063/1.1710092

[34] Weaver, S.C. (1972) An Investigation of the Thermal Conductivity, Electrical Resistivity, and Thermoelectric Power of Thorium Nitride-Uranium Nitride Alloys. Ph.D. Thesis, University of Tennessee.

[35] Gerardin, M., Gilabert, E., Horlait, D., Barthe, M. and Carlot, G. (2021) Experimental Study of the Diffusion of Xe and Kr Implanted at Low Concentrations in UO_2 and Determination of Their Trapping Mechanisms. *Journal of Nuclear Materials*, **556**, Article 153174. https://doi.org/10.1016/j.jnucmat.2021.153174